Eur J Nucl Med Mol Imaging (2008) 35:611–623
DOI 10.1007/s00259-007-0554-7

ORIGINAL ARTICLE

Iodine-124 PET dosimetry in differentiated thyroid cancer: recovery coefficient in 2D and 3D modes for PET(/CT) systems

Walter Jentzen · Reiner Weise · Jürgen Kupferschläger · Lutz Freudenberg · Wolfgang Brandau · Ronald Bares · Wolfgang Burchert · Andreas Bockisch

Received: 9 January 2007 / Accepted: 25 July 2007 / Published online: 10 October 2007

Abstract
Purpose This study evaluated the absolute quantification of iodine-124 (^{124}I) activity concentration with respect to the use of this isotope for dosimetry before therapies with ^{131}I or ^{131}I-labeled radiotherapeuticals. The recovery coefficients of positron emission tomography(/computed tomography) PET(/CT) systems using ^{124}I were determined using phantoms and then validated under typical conditions observed in differentiated thyroid cancer (DTC) patients.
Methods Transversal spatial resolution and recovery measurements with ^{124}I and with fluorine-18 (^{18}F) as the reference were performed using isotope-containing line sources embedded in water and six isotope-containing spheres 9.7 to 37.0 mm in diameter placed in water-containing body and cylinder phantoms. The cylinder phantom spheres were filled with ^{18}F only. Measurements in two-dimensional (2D) and three-dimensional (3D) modes were performed using both stand-alone PET (EXACT HR$^+$) and combined PET/CT (BIOGRAPH EMOTION DUO) systems. Recovery comparison measurements were additionally performed on a GE ADVANCE PET system using the cylinder phantom. The recovery coefficients were directly determined using the activity concentration of circular regions of interest divided by the prepared activity concentration determined by the dose calibrator. The recovery correction method was validated using three consecutive scans of the body phantom under our ^{124}I PET(/CT) protocol for DTC patients.
Results Compared with that of ^{18}F, transversal spatial resolution of ^{124}I was slightly, but statistically significantly degraded (7.4 mm *vs.* 8.3 mm, $P<0.002$). Using the body phantom, recovery was lower for ^{124}I than for ^{18}F in both 2D and 3D modes. The ^{124}I recovery coefficient of the largest sphere was significantly higher in 2D than in 3D mode (81% *vs.* 75%, $P=0.03$). Remarkably, the ^{18}F recovery coefficient for the largest sphere significantly deviated from unity (range of 87%–93%, $P<0.004$) for all scanners but the GE ADVANCE. The maximum range of inaccuracy of the measured ^{124}I activity concentration under *in vivo* conditions after applying partial volume correction was ±10% for spheres ≥12.6 mm in diameter.
Conclusions Recovery correction is mandatory for ^{124}I PET quantification, even for large structures. To ensure accurate dosimetry, thorough absolute recovery measurements must be individually established for the particular PET scanner and radionuclide to be used.

Keywords Partial volume effect · PET · Dosimetry · Iodine-124 · Thyroid cancer

W. Jentzen (✉) · L. Freudenberg · W. Brandau · A. Bockisch
Klinik für Nuklearmedizin, Universität Duisburg-Essen,
Hufelandstrasse 55,
45122 Essen, Germany
e-mail: walter.jentzen@uni-duisburg-essen.de

R. Weise · W. Burchert
Institut für Radiologie, Nuklearmedizin und Molekulare Bildgebung, Herz- und Diabeteszentrum NRW,
Georgstrasse 11,
32545 Bad Oeynhausen, Germany

J. Kupferschläger · R. Bares
Klinik für Nuklearmedizin, Universität Tübingen,
Röntgenweg 13,
72076 Tübingen, Germany

Introduction

Iodine-124 positron emission tomography (^{124}I PET) lately has emerged as an attractive modality for lesion dosimetry prior to (^{131}I) radioiodine therapy of differentiated thyroid

cancer (DTC) [1–6]. For accurate dosimetry, the absolute activity concentration in the lesion must be measured reliably. Correction must be made for the partial recovery effect, namely, every PET scanner's systematic underestimation of activity in lesions smaller than two to three times the scanner resolution [7–9]. To accomplish such correction, one must determine both in two-dimensional (2D) and three-dimensional (3D) modes the absolute recovery coefficient of ^{124}I. This value is calculated by dividing the activity concentration of (test) objects of various sizes as determined by the scanner by the activity concentration of the same objects measured by, for instance, a well counter.

To optimize the accuracy of PET with ^{124}I, the complex decay scheme of this radionuclide also must be taken into account. This decay scheme includes a cascade gamma radiation coincidence, which, for instance, increases spurious activity and decreases image contrast of ^{124}I PET relative to PET using the pure positron emitter, fluorine-18 (^{18}F) [10, 11]. Only a limited number of phantom studies [11–14] on different PET scanners were performed to establish ^{124}I quantitative imaging. To our knowledge, none of these studies has reported absolute rather than relative recovery coefficients and none has used ^{18}F as a gold standard for accuracy.

We therefore performed the present prospective study to determine the absolute recovery coefficients of the University of Duisburg-Essen Nuclear Medicine Clinic's standalone PET and combined PET/computed tomography (CT) systems using ^{124}I. To delineate the effect of cascade gamma rays, we also scanned our phantoms using ^{18}F as a reference. Moreover, we validated the resultant recovery correction coefficient under typical conditions observed in DTC patients by performing three consecutive scans under our clinical whole-body protocol. The prospective study unexpectedly observed a significant underestimation of absolute ^{18}F activity in objects far larger than the threshold size for the partial recovery effect. To assess whether this error was institution- or system-specific, we performed an additional exploratory study with the same model of scanner in another institution as well as a scanner from another manufacturer. In the present publication, we report the results of both the prospective and exploratory studies.

Materials and methods

Figure 1 illustrates the design of our prospective and exploratory studies. Methodological details are given below.

Radionuclides

^{18}F was obtained from a Cyclone 18/9 (IBA, Louvain-la-Neuve, Belgium) according to standard methodology. ^{124}I was produced in the CV 28 cyclotron (Cyclotron Corporation, Berkeley, CA, USA) and purified under methods described in detail elsewhere [15, 16].

Calibrated activity measurement—dose calibrator and well counter

Using the dose calibrator, high activities of ^{124}I or ^{18}F were measured using a CRC®-15R dose calibrator (Capintec Inc.,

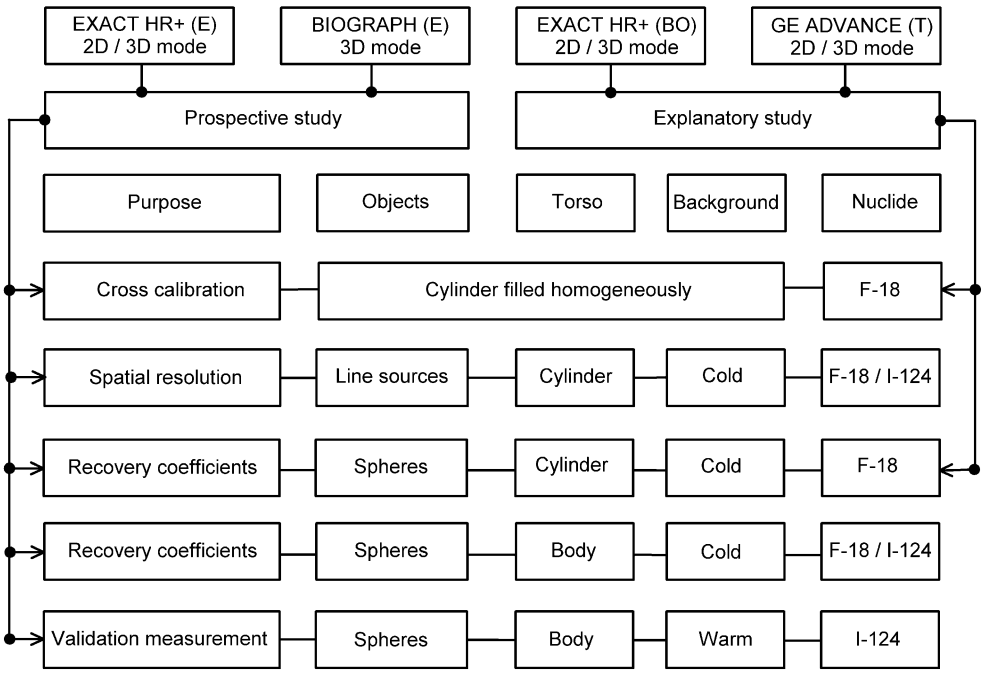

Fig. 1 Illustration of the study design. The PET systems examined were located at the universities in Essen (E), Bad Oeynhausen (BO), and Tübingen (T), Germany. The study comprised prospective and explanatory parts using phantoms with different objects filled with ^{124}I or ^{18}F as reference

Ramsey, NJ, USA). The samples were placed in a P6 vial (Amersham International, Buckinghamshire, UK) containing 1 ml of radioactive solution. For ^{124}I, the dose calibrator was calibrated by cross-validation of a sample activity with the measurements of the Physikalisch-Technische Bundesanstalt (PTB), the institution in Germany responsible for national radiation measurement standards. Additionally, both the ^{124}I and ^{18}F activities were checked via gamma spectroscopy (Genie 2000 software, Canberra, Australia).

The well counter (1480 Wallac Wizard; Perkin-Elmer, Wellesley, MA, USA) was calibrated based on the activity measurements displayed by the CRC®-15R dose calibrator. The well counter's linearity (count rate *vs*. activity) was checked for the activity ranges to be used in the phantom measurements. Under conditions identical with those of the calibration measurements, the well counter was used to measure small activities, such as aliquots obtained from the spheres placed inside the phantoms or from phantom cavities. These samples were placed in a 2-ml vial containing 1 ml of radioactive solution.

PET tomographs

For the prospective study (Fig. 1), PET imaging was performed using two (ECAT) EXACT HR$^+$ PET scanners at the University of Duisburg-Essen Nuclear Medicine Clinic: one a stand-alone system (CTI/Siemens, Erlangen, Germany), which images in both 2D and 3D modes [17], and the other the PET component of a combined PET/CT scanner, the BIOGRAPH EMOTION DUO (Siemens Medical Solutions, Hoffman Estates, IL, USA), which lacks septa and therefore images in 3D only [18].

The exploratory study (Fig. 1) used a second stand-alone EXACT HR$^+$ with both 2D and 3D imaging capabilities from the Institute of Radiology, Nuclear Medicine and Molecular Imaging of the Heart and Diabetes Center of Nordrhein-Westphalia, Bad Oeynhausen, Germany. Additionally, the exploratory study employed a stand-alone PET scanner of another model and manufacturer (GE ADVANCE; General Electric Medical Systems, Milwaukee, WI, USA) from the University of Tübingen Nuclear Medicine Clinic, which images in both 2D and 3D modes [19, 20].

The EXACT HR$^+$ PET system consisted of 32 rings (63 image planes with a plane separation of 2.43 mm). The energy window ranged from 350 to 650 keV (2D and 3D mode). The GE ADVANE PET system consisted of 18 rings (35 image planes with a plane separation of 4.25 mm). The energy window ranged from 300 to 650 keV in 2D and 375 to 650 keV in 3D mode. The axial field-of-view (FOV) was 15.2 cm for both the EXACT HR$^+$ and GE ADVANCE systems.

CT tomograph and scanning parameters

The CT component of the BIOGRAPH combined PET/CT scanner was a dual-slice spiral CT scanner. All CT scans were performed using a 130 kVp tube voltage, 130 mAs, a 3 mm per rotation table speed, and a 3-mm slice width, except that an 8 mm per rotation table speed and a 5-mm slice width were used in the scans performed to validate our recovery correction methods under typical clinical conditions.

PET tomograph calibration

Because of the unexpected result in the prospective study, the PET calibration will be described thoroughly. Before any phantom measurements were performed, the PET scanners underwent a complete normalization including gantry setup to equalize the detector photomultiplier tube gains and energy thresholds, adjustment for relative efficiency variations, and calibration to enable quantitative measurements. The branching ratios for the PET tracers used were 0.97 (^{18}F) and 0.23 (^{124}I) [21]. Cross-calibrations between each PET system and the dose calibrator or well counter were performed using ^{18}F. PET systems were calibrated in 2D or 3D mode using a standard cylindrical reference phantom (20 cm axial length, 20-cm outside diameter, 6.265 l inside volume measured by fluid displacement). This phantom was filled with ^{18}F activities according to the manufacturer's recommendations. The activity concentration was determined using the dose calibrator and aliquots of the phantom contents in the well counter. The phantom was placed on the dedicated holder provided by the manufacturer and located centrally within the FOV.

A "cold" transmission scan (acquisition time 120 min) was acquired on the stand-alone PET systems for attenuation correction using cold water (no radioactivity) in the phantom during transmission measurements. The attenuation correction of the BIOGRAPH PET system was based on the CT images; therefore, the measurements started with a spiral CT scan of the cylinder when this phantom already was filled with the ^{18}F activity. The emission scans were acquired for 120 min in 2D mode and 60 min in 3D mode. The emission and transmission images were reconstructed with standard filtered backprojection (FBP) with a 5-mm Gaussian filter. The measured attenuation map after segmentation was used for attenuation correction. The analysis was based on circular regions of interest (ROIs) drawn centrally over the transversal plane with a 17-cm diameter. Only a distance of about ±6.5 cm in the axial direction from the middle of the phantom was considered in the determination of the average activity concentration. The PET calibration factors were adjusted appropriately.

There were two items worth mentioning. First, selecting a circular ROI that equalled the actual diameter of the cylinder phantom (20 cm) resulted in 5% increase of the calibration factor, which was caused by edge effects (intensity drop at the edges). Second, it would seem suitable to perform cross-calibration using the non-pure positron emitter ^{124}I instead of the pure positron emitter ^{18}F. The resulting calibration factors would be specific for the radionuclide used. Use of ^{124}I for cross-calibration probably gives rise to a significant amount of spurious activity introduced by cascade gamma rays that is not removed in the standard software packages of PET systems suppliers, leading to a seemingly increased PET activity in the cylinder phantom, particularly in 3D mode. In the present study, measurements on the PET systems calibrated with ^{18}F corroborated this suggestion. Filling the cylinder phantom with known prepared activity concentration of ^{124}I resulted in an overestimation of the measured ^{124}I activity concentration of 8% in 3D mode; however, the measured activity was accurate in 2D mode (1%).

Phantoms and their preparation

Resolution phantom For the phantom for measuring the transversal spatial resolution, transversal (in-plane) spatial resolution (x, y) in water was measured in two directions (radially and tangentially) using a line source orthogonal to the transverse plane that was embedded in the cylinder phantom (20-cm axial length, 20-cm outside diameter) filled with cold water. The line source, consisting of polyethylene tubing (0.8-mm inner diameter, 1.6-mm outer diameter), was looped back through the phantom to provide distances of 1 cm and 7 cm from the central axis of the FOV. The transversal spatial resolution was measured at four positions each at the center (z=0) and one-fourth of the axial FOV (z=±1/4 FOV), *i.e.*, (x=1 cm, y=0), (x=7 cm, y=0), (x=0, y=1 cm) and (x=0, y=7 cm). The line source was filled with either ^{124}I or ^{18}F. These measurements were performed on the Essen EXACT HR$^+$ and BIOGRAPH PET systems only.

Recovery phantoms The National Electrical Manufacturers Association (NEMA)/International Electrotechnical Commission (IEC) 2001 body phantom (elliptically shaped torso phantom) without a lung insert [22, 23] and a cylinder phantom (20 cm in axial length, 20-cm outside diameter) were used as recovery phantoms. For the recovery measurements, both these phantoms contained six refillable spheres of different sizes. The inner diameters (volumes) of the spheres were: 9.7 mm (0.47 ml), 12.6 mm (1.05 ml), 17.1 mm (2.60 ml), 22.2 mm (5.75 ml), 28.0 mm (11.44 ml), and 37.0 mm (26.53 ml).

The spheres in the body phantom were filled from a stock solution of ^{124}I or ^{18}F to measure the "hot" spot recovery coefficients (radioactivity-containing spheres in a cold background) for the Essen EXACT HR$^+$ and BIOGRAPH PET systems. In the present paper, the activity concentration measured using the dose calibrator is referred to as the "prepared" activity concentration, whereas the activity concentration obtained from the PET image is termed the "measured" activity concentration. The prepared ^{18}F sphere activity concentration was about 80 kBq/ml in 2D and 40 kBq/ml in 3D mode; the prepared ^{124}I sphere activity concentration was about 60 kBq/ml in both modes. The phantom cavities were filled with water only.

The spheres in the cylinder phantom were filled with ^{18}F only to measure the hot spot recovery coefficients for not only the Essen EXACT HR$^+$ and BIOGRAPH scanners (prospective study), but for another EXACT HR$^+$ located at a different institution in Bad Oeynhausen (BO) and for a PET system from another manufacturer, namely the GE ADVANCE (exploratory study) located in Tübingen (T). The prepared ^{18}F sphere activity concentration was about 80 kBq/ml in 2D mode and 40 kBq/ml in 3D mode.

Validation phantom To validate the recovery correction method that was derived in the prospective study, the body phantom was used with ^{124}I-containing spheres only to mimic *in vivo* conditions seen in DTC patients. Validation was performed with the Essen EXACT HR$^+$ and BIOGRAPH PET systems only. Based on our standard administered ^{124}I activity of about 30 MBq [6] to patients and the 70 kg weight of a standard adult human, the torso activity concentration ought to be about 0.43 kBq/ml, assuming homogeneous activity distribution and a tissue density of 1 g/ml. For the spheres a concentration of about 50 kBq/ml [6] was used that falls within the concentration range of ^{124}I-accumulating lesions at 24 h. This concentration coincided with the NEMA protocol for ^{18}F. In the phantom measurement, the prepared activity concentrations were 43.12 kBq/ml for the sphere and 0.44 kBq/ml for the torso. The resulting prepared source-to-background ratio was therefore 98 as directly checked with the well counter using aliquots obtained from spheres and the phantom cavity, *i.e.*, nearly pure hot spot imaging.

PET(/CT) acquisition protocol

For the acquisition for transversal spatial resolution determination, the phantoms were placed centrally within the FOV. For the Essen EXACT HR$^+$ stand-alone PET, a cold 60-min transmission scan was acquired before the line source were filled with radioactivity. BIOGRAPH measurements started with a spiral CT scan with the

activity already filled in the line source. The emission scans lasted 2 h each in 2D and 3D mode.

For the acquisition for recovery coefficient determination, the acquisitions were performed with high statistical precision. The acquisition parameters for the body and cylinder phantoms were identical. For the three stand-alone PETs (Essen and Bad Oeynhausen EXACT HR$^+$ scanners, GE ADVANCE scanner), a cold 180-min transmission scan was acquired before the spheres were filled with radioactivity. The total ^{68}Ge/^{68}Ga rod source activity was 240 MBq (EXACT HR$^+$) or 550 MBq (GE ADVANCE) at the time of measurement. Two emission scans each were acquired successively in 2D and 3D modes. The ^{18}F emission scans lasted 2 h in 2D and 1 h in 3D mode. The ^{124}I emission scans lasted 3 h in both modes. BIOGRAPH measurements started with a spiral CT scan with the activity already filled into the spheres. For the EXACT HR$^+$ component of the BIOGRAPH, ^{18}F emission scans lasted 2 h and ^{124}I emission scans lasted 3 h. In addition, the PET calibration factors on the scanners were checked with subsequent measurements using a standard reference cylinder provided by the manufacturer that was homogeneously filled with ^{18}F.

The phantom acquisition for validation of the recovery correction method was identical with our typical whole-body PET(/CT) patient measurement. On the Essen EXACT HR$^+$ PET system, the durations of the emission (transmission) scans were 480 s (240 s) in 2D mode and 281 s (138 s) in 3D mode. BIOGRAPH measurements started with a whole-body spiral CT scan. After completion of this scan, the bed was advanced automatically to the PET and one-bed emission began. The emission scan lasted 300 s. Three consecutive scans were performed.

Image reconstruction

The phantom images were reconstructed using the typical patient's iterative image reconstruction algorithm. The image reconstruction was performed after Fourier rebinning with attenuation-weighted ordered-subset expectation maximization (AW-OSEM) using two iterations, eight subsets, and a 5-mm Gaussian filter. The data were corrected for attenuation by measured ^{68}Ge/^{68}Ga transmission including image segmentation in PET, while PET/CT used the CT-based attenuation correction approach. Standard scatter correction in 2D and 3D modes was implemented in the PET(/CT) system. The resulting PET images of the body and cylinder phantoms had 128×128 voxels, and those of the transversal spatial resolution phantom had 512×512 voxels. The voxel size of the images of the body and cylinder phantom was 1.72×1.72×2.43 mm^3 (EXACT HR$^+$ and BIOGRAPH) or 2.34×2.34×4.25 mm^3 (GE ADVANCE). The voxel size of the images of the transversal spatial resolution phantom was 0.43×0.43×2.43 mm^3 for the Essen EXACT HR$^+$ and BIOGRAPH PET systems.

The above OSEM 2×8 reconstruction with image segmentation was used as the default. To evaluate the specific degree to which differences in the recovery coefficients and transversal spatial resolution were related to image reconstruction, additional analysis was performed. Images were reconstructed using OSEM reconstructions with various numbers of iterations and subsets (OSEM 1×32 and OSEM 4×16) and standard FBP. The images were smoothed with a 5-mm Gaussian filter. For recovery curves, this additional analysis was performed for the BIOGRAPH PET system only. For the transversal spatial resolution, the analysis was performed on both the Essen EXACT HR$^+$ and BIOGRAPH PET systems.

Images were reconstructed with the software packages ECAT 7.2.1 (Essen and Bad Oeynhausen EXACT HR$^+$), Syngo Somaris/5, VA40C (BIOGRAPH), and ADVANCE release 6.0 (GE ADVANCE).

Data analysis

Transversal spatial resolution The image spatial resolution was expressed as full width at half maximum (*FWHM*). The width of the reconstructed line spread function in the tangential and radial directions was measured for each line source position. These line profiles were fitted with a Gaussian function. The average value (n=12) in the tangential and radial directions obtained at transversal (1 cm and 7 cm) and axial positions (center and ±1/4 FOV) are given. Images and data were analyzed with PMOD 2.5 software (PMOD Technologies Ltd., Zurich, Switzerland) and PeakFit 4.0 (Jandel Scientific, San Rafael, CA, USA).

Activity concentration The activity concentration was measured using circular ROIs with an 8-mm diameter (*FWHM*-sized ROIs) as suggested by others [9, 23]. These ROIs were positioned at the apparent center of the sphere, and the mean of the voxels in the *FWHM*-sized ROI was calculated. The transversal planes were used for analysis. For spheres with an inner diameter >17.1 mm, the average ROI value was calculated from adjacent planes (±1). The concentrations of spheres with an inner diameter ≤17.1 mm were obtained using a line profile (the mean of the *FWHM*-sized ROIs *vs*. axial distance) around the maximum. The line profile was fitted with a Gaussian function and the Gaussian amplitude was taken as the activity concentration. Images were analyzed with PMOD 2.5 software.

Recovery coefficient and error analysis The absolute measured recovery coefficients were directly calculated using

the measured activity concentration of the *FWHM*-sized ROI of 8 mm (see above) divided by the prepared activity concentration as determined by the well counter. The resulting recovery curves were parameterized using a three-parameter sigmoid function: $RC(d) = \alpha\left[1 + (\gamma/d)^{\beta}\right]^{-1}$. The symbol *RC* indicates the size-dependent recovery coefficient, d is the diameter of the sphere, and α, β, γ are fitting parameters.

Different sources of error occurred in the determination of the recovery coefficients. First, the estimated relative standard deviation (*RSD*), RSD_{ROI}, of the mean value in the *FWHM*-sized ROI (each containing n=15 voxels) including ROI placement was larger for the smallest spheres than for the largest sphere (≈7% *vs.* ≈1%). Second, the uncertainty of cross calibration was another source of error. PET calibration factors were checked after each recovery measurement. The error of the cross-calibration was estimated by nine calibration measurements. The mean relative deviation between the measured and prepared activity concentrations in the cylinder was 0.8% and the corresponding RSD_{Cross} was ±2.2%. Third, the last error was associated with the activity concentration measurement of the aliquots of the phantom spheres in the well counter. The mean relative deviation between the dose calibrator and well counter estimated by repeated measurements (n=9) was 0.9% and the corresponding RSD_{Counter} was ±1.0%. The total error estimate, ΔRC, according to Gaussian error propagation law was $\Delta RC = RC \cdot \sqrt{RSD^2_{\mathrm{ROI}} + RSD^2_{\mathrm{Cross}} + RSD^2_{\mathrm{Counter}}}$. In the figures, the uncertainties are displayed as vertical error bars around each data point.

Recovery correction method For a large source-to-background ratio, *i.e.,* nearly pure hot spot imaging, the corrected activity concentration, C_{cor}, can be estimated with $C_{\mathrm{cor}} = C_{\mathrm{msd}}/RC$ [24]. The measured activity concentration, C_{msd}, was obtained using circular ROIs with a diameter of 8 mm (*FWHM*-sized ROI). The procedure was identical with the determination of the recovery coefficient as described above. The torso activity concentration (background) was determined using circular ROIs with a 16-cm diameter drawn on planes on which the spheres were not visible, but excluding the first and last five planes and using additional circular ROIs with a 4-cm diameter located in the center of the torso phantom cavity containing the spheres. The mean of the 53 ROIs was taken as the torso activity concentration. For each whole-body scan, the corrected activity concentration of each sphere was determined using the recovery coefficients obtained from the parameterized recovery curve. The individual percentage deviations between the recovery-corrected and prepared activity concentrations (physical decay corrected to the first scan) were calculated for each sphere.

Statistical analysis The errors of the measured quantities were assumed to be normally distributed. The two-sided Z value for a difference was used to compare recovery coefficients, *FWHM* values, and source-to-background ratios. For all statistical analyses, a P value <0.05 was considered statistically significant (*i.e.*, a Z value equal to 1.96 or 95% confidence interval).

Results

Transversal spatial resolution

Table 1 lists the results of the transversal spatial resolution measurements, which represent the transversal image resolution in clinical applications. No significant differences were noted between results obtained with the two acquisition modes or image reconstruction methods. The mean ± standard deviation (*SD*) *FWHM* was 8.3±0.2 mm for ^{124}I and 7.4±0.2 mm for ^{18}F; these values differed significantly (P<0.002). A small degree of resolution degradation of 1 mm was noted for ^{124}I *vs.* ^{18}F.

Recovery coefficients

The absolute hot spot recovery coefficients of the body phantom are shown in Figs. 2, 3, and 4 (Essen EXACT HR$^+$ and BIOGRAPH). Table 2 summarizes the recovery coefficients of the 37-mm spheres as an example of a large object.

Recovery was lower with ^{124}I than with ^{18}F. Based on the individual values of the spheres, the mean ± *SD* decreases relative to ^{18}F were −12.7±4.6% in 2D, −12.4±4.8% in 3D (Essen EXACT HR$^+$), and −13.8±5.6% in 3D (BIOGRAPH). The measured ^{124}I recovery coefficients for the 37-mm sphere were 81% in 2D and 75% in 3D mode (Essen EXACT HR$^+$) and 77% in 3D mode (BIOGRAPH). Hence, the ^{124}I recovery for large objects was higher in 2D than in 3D mode; this difference was statistically significant (P=0.03).

Table 1 Average transversal spatial resolution (*FWHM** in mm, *SD*† ±0.2 mm) in water under different image reconstruction methods and acquisition modes for ^{124}I (^{18}F)

	EXACT HR$^+$, 2D	EXACT HR$^+$, 3D	BIOGRAPH, 3D
FBP	8.6 (7.6)	8.4 (7.6)	8.6 (7.5)
OSEM 2×8	8.1 (7.3)	8.0 (7.2)	8.2 (7.4)
OSEM 1×32	8.3 (7.4)	8.2 (7.4)	8.4 (7.5)
OSEM 4×16	8.3 (7.3)	8.2 (7.4)	8.4 (7.5)

**FWHM*, full width at half maximum. † *SD*, standard deviation.

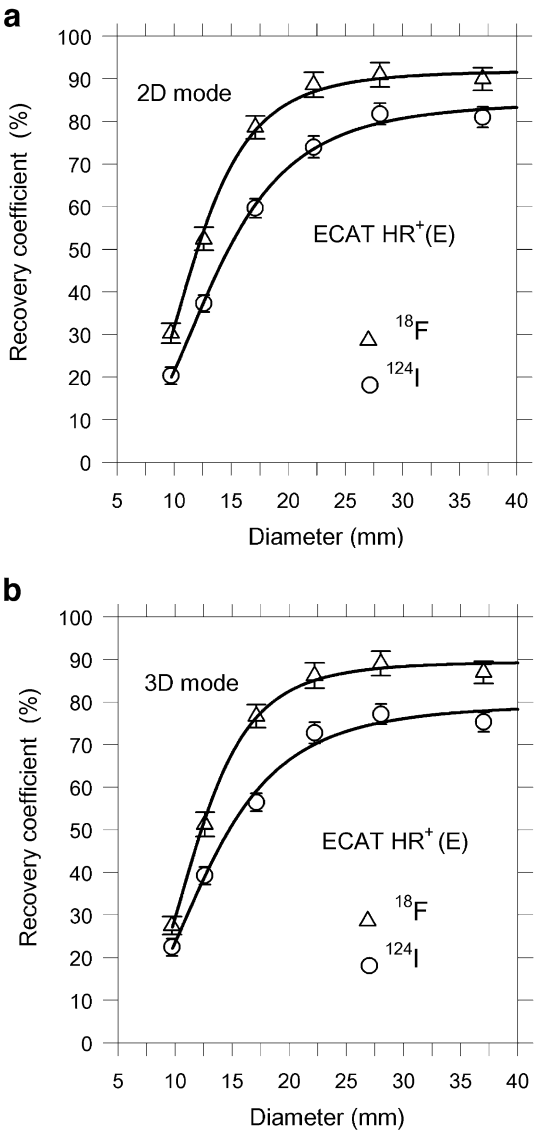

Fig. 2 Absolute recovery coefficients of ^{124}I and ^{18}F for EXACT HR$^+$ PET system located in Essen (E) measured with a body phantom containing radionuclide-filled spheres, acquired in 2D (**a**) or 3D (**b**) modes. Analysis was based on 8-mm *FWHM*-sized ROIs. Image reconstruction was performed after Fourier rebinning (AW-OSEM at two iterations and eight subsets with a 5-mm Gaussian filter). The sizes of the error bars indicate the uncertainty (see text). The data points were fitted using a three-parameter sigmoid function (solid line)

The recovery curves obtained from images reconstructed with various OSEM parameters and FBP are depicted in Fig. 3 for ^{124}I and Fig. 4 for ^{18}F. Recovery coefficients were larger for the OSEM- than for the FBP-reconstructed images, except in the case of the largest (37-mm) sphere, for which the recovery coefficients were identical using both algorithms (maximum deviation from FBP: ±1.5%). Based on the individual values for the spheres with diameters <37 mm, the mean ± *SD* observed recovery increase for OSEM relative to FBP was 11.4±5.6% for ^{18}F and 7.5±4.2% for ^{124}I. For most spheres, recovery values obtained within OSEM were similar regardless of the iteration and subset parameters. However, for the 22.2-mm and 28.0-mm spheres, recovery values appeared be about 5% larger for OSEM 2×8 than for OSEM 1×32 or OSEM 4×16.

The observed ^{18}F recovery coefficients of the body phantom for large objects were 90% in 2D and 87% in 3D mode (Essen EXACT HR$^+$) and 89% in 3D mode (BIOGRAPH). The differences in 2D and 3D mode were not significant, but the measured ^{18}F recovery coefficient for the 37-mm sphere significantly deviated from full recovery (P<0.001) regardless of the image reconstruction method used. Because of this unexpected finding, the scatter geometry of the phantom was changed through the substitution of a cylinder phantom for the body phantom [9]. Identical spheres were used with either phantom. Figure 5 shows the resulting ^{18}F recovery coefficients. These recovery coefficients did not significantly differ from those obtained using the body phantom (Table 2). With the cylinder phantom, full recovery again was not reached (P<0.001).

We therefore performed an exploratory study measuring ^{18}F recovery coefficients using the cylinder phantom and another EXACT HR$^+$ PET system located in Bad Oeynhausen, Germany, or a PET system from a different manufacturer (GE ADVANCE) operated in Tübingen, Germany. The default OSEM reconstruction was used for the EXACT HR$^+$ PET system. However, the data from the GE ADVANCE were reconstructed using OSEM 4×16 because the regions reconstructed with OSEM 2×8 using GE ADVANCE software had not reached the convergence compared with its FBP-reconstructed images. This effect was attributed to the manufacturer-specific implementation of the OSEM algorithm. The recovery curves from the exploratory study are shown in Figs. 6 and 7, and the measured recovery coefficients for the 37-mm sphere are listed in Table 2. Almost full recovery was reached for the GE ADVANCE, but again not for the EXACT HR$^+$ PET system (P<0.004).

Validation of recovery correction method

The individual percentage deviations between the recovery-corrected and the prepared activity concentrations are given in Table 3. Using all spheres, the mean relative deviation ± *SD* between recovery-corrected and prepared sphere concentrations were −0.5%±6.0% in 2D and −3.5%±5.3% in 3D mode for Essen EXACT HR$^+$ and −3.2%±11.0% in 3D mode for the BIOGRAPH PET system. The results of repeatability measurements including recovery correction indicated that, except for the smallest spheres, the range of uncertainty of the mean recovery-corrected activity concentrations was ±10%. The reproducibility of the smallest

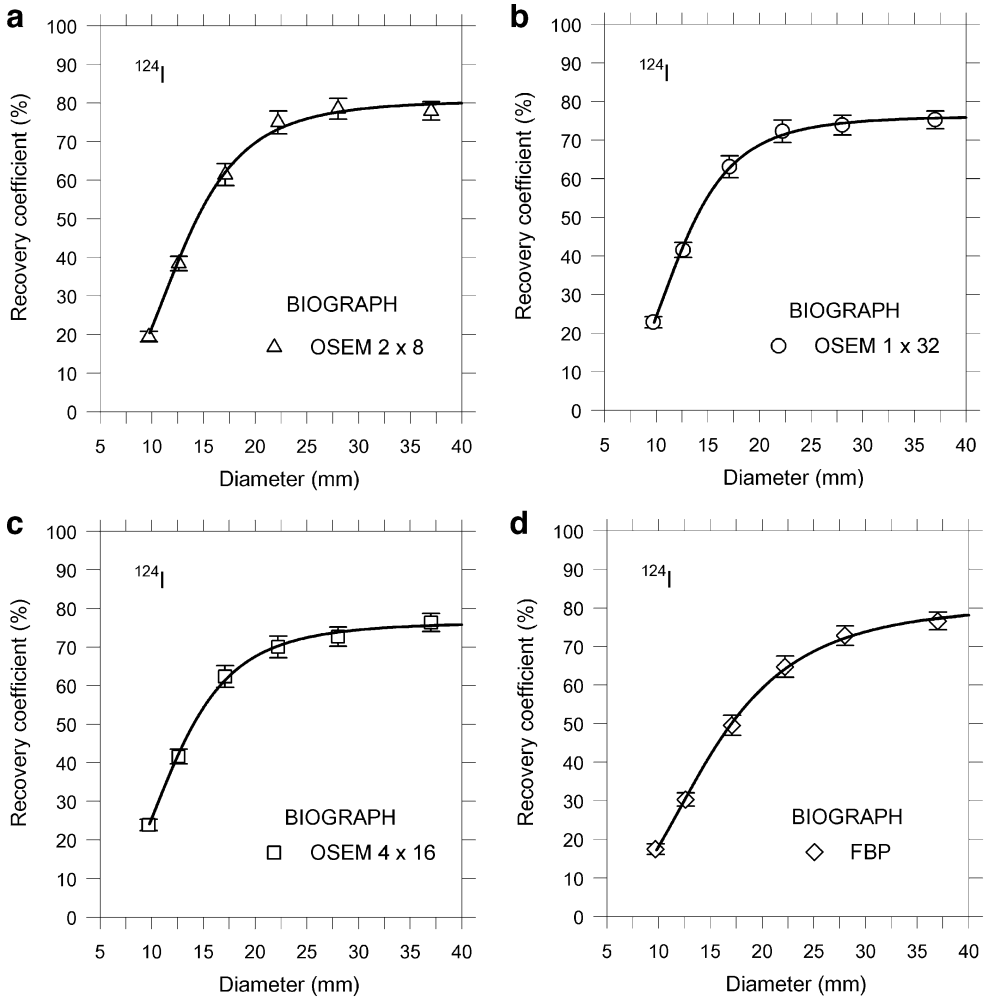

Fig. 3 Absolute recovery coefficients of ^{124}I for the BIOGRAPH PET system measured with a body phantom containing radionuclide-filled spheres, acquired in 3D mode: (**a**) OSEM 2×8, (**b**) OSEM 1×32, (**c**) OSEM 4×16, (**d**) FBP. Methodology is described in the caption of Fig. 2

sphere was inferior. In particular with BIOGRAPH PET imaging, the mean relative deviation was −21%.

The measured activity concentrations at start time derived from the images using the 37-mm sphere were 35.5 kBq/ml in 2D and 32.9 kBq/ml (Essen EXACT HR$^+$) and 32.1 kBq/ml (BIOGRAPH) in 3D mode. The measured mean torso activity concentrations at start time ± *SD* was 0.62±0.37 kBq/ml in 2D and 0.74±0.33 kBq/ml in 3D mode for the Essen EXACT HR$^+$ and 0.69±0.20 kBq/ml in 3D mode for the BIOGRAPH PET system. The corresponding measured source-to-background ratios were therefore 57 (EXACT HR$^+$, 2D), 45 (EXACT HR$^+$, 3D), and 47 (BIOGRAPH, 3D). The measured source-to-background ratios significantly deviated from the prepared source-to-background ratio in 3D (P<0.01), but did not in 2D mode. The background increase can be mainly attributed to the presence of spurious activities due to gamma-decay cascades of ^{124}I resulting in decrease of image contrast [11].

Discussion

For an accurate representation of the tracer concentration, the voxel counts in images must be related to the actual concentration via a constant PET calibration factor. Partial volume effects cause this calibration factor to depend on the size and shape of the imaged object: the measured activity concentration is underestimated for an object (*i.e.*, lesion) with a diameter smaller than two to three times the scanner resolution [7–9]. Thus, along with image contrast (and therefore tracer specificity), spatial resolution is a major limiting factor for accurate quantification. Nonetheless, partial volume effects can be corrected for using empirically obtained recovery coefficients.

These recovery coefficients are generally derived from experiments with physical objects. These empirical methods mimic the object imaged in clinical practice by using simple geometrical shapes such as cylinder or spheres. In

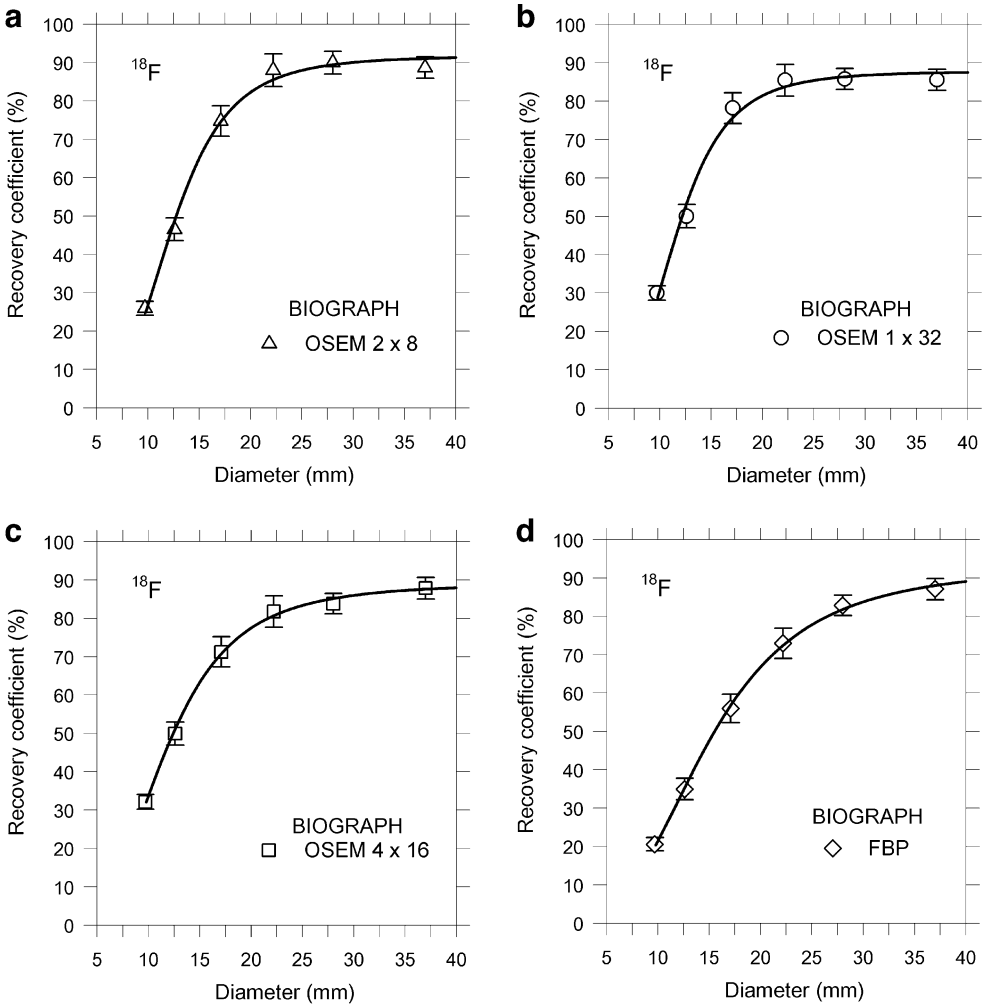

Fig. 4 Absolute recovery coefficients of ^{18}F for the BIOGRAPH PET system measured with a body phantom containing radionuclide-filled spheres, acquired in 3D mode: (**a**) OSEM 2×8, (**b**) OSEM 1×32, (**c**) OSEM 4×16, (**d**) FBP. Methodology is described in the caption of Fig. 2

PET tumor imaging such as ^{18}F-fluorodeoxyglucose or ^{124}I PET, it is generally accepted that, in a first approximation, the shape of the lesions can be described by a sphere model and the activity distribution is assumed to be homogenous. Under these assumptions, recovery correction requires one measurement using a phantom with spheres of known diameters and activity concentrations (lesion and background) that closely mimic *in vivo* conditions [24].

The absolute recovery curves that we obtained for ^{124}I and ^{18}F are shown in Figs. 2, 3, 4, 5, 6, 7. The spatial resolution in PET depends on the positron energy of the isotope of interest [25]. The recovery of the non-pure positron emitter ^{124}I (maximum positron energy: 2.14 MeV) is expected to be inferior to the recovery of the pure positron emitter ^{18}F (maximum positron energy: 0.63 MeV) [14]. In fact, the recovery for EXACT HR^{+} and BIOGRAPH PET systems was indeed lower for ^{124}I than for ^{18}F. The measured line-spread functions (a common measure of the spatial resolution) were, however, similar for both isotopes. The observed degradation in transversal resolution was only 1 mm (Table 1), which agrees with published data [14]. This finding suggests that the observed degradation of the ^{124}I recovery coefficient is not only associated with the longer range of the more energetic ^{124}I positron relative to that of the ^{18}F positron, but mainly with the complex decay scheme of ^{124}I. ^{124}I emits gamma rays that are in cascade with the emitted positron, a phenomenon that often results in spurious coincident photon pairs. The impact of these spurious coincidences is expected to create greater inaccuracy in 3D than in 2D mode if no correction method is applied [10]. Using the standard PET reconstruction software, measurements on the EXACT HR^{+} and BIOGRAPH PET systems confirmed this expectation: the ^{124}I recovery coefficients were slightly inferior in 3D *vs*. 2D mode (Fig. 2).

The recovery coefficient of the pure positron emitter ^{18}F should converge to 100% for objects larger than two to three times the scanner resolution and decrease significantly for objects smaller than this [7–9]. As shown in Figs. 2, 3,

Table 2 Absolute hot spot recovery coefficients (in %) for ^{18}F (^{124}I) for an object (37-mm sphere) far larger than the threshold size for partial recovery effect*

Scanner	Cylinder phantom		Body phantom	
	2D	3D	2D	3D
EXACT HR$^+$ (E)	91†	89†	90† (81‡)	87† (75‡)
BIOGRAPH (E)	–	87†	–	89† (77)
EXACT HR$^+$ (BO)	89†	93†	–	–
GE ADVANCE (T)	97	99	–	–

*Recovery coefficients for scanners located in Essen (E), Bad Oeynhausen (BO), and Tübingen (T). OSEM 2×8 image reconstruction was used, except for GE ADVANCE that used OSEM 4×16 (see text). † Significant difference from full recovery for ^{18}F, $P<0.004$. ‡ Significant difference between 2D and 3D mode, $P=0.03$.

4, 5, 6, 7, the asymptotic behavior of the recovery curves is clearly visible and the recovery coefficients significantly decrease for spheres with diameters ≤22.2 mm (about two to three times the scanner resolution) for both ^{18}F and ^{124}I. The curvature of the recovery curves is therefore in good agreement with theoretical considerations and experiments [7–9]. However, the absolute value of the ^{18}F recovery coefficients for the 37-mm sphere as an example of a large object (four to five times the scanner resolution) significantly deviated from 100% for both the body and cylinder phantoms on EXACT HR$^+$ operated at two different institutions and BIOGRAPH PET/CT system (Table 2). This unexpected result for ^{18}F was still observed after recalculating the recovery coefficient using the rescaled ^{18}F activity concentration of the reference cylinder (a reference for a large object) as recommended by other authors [9, 24]. Our results cannot be compared with those of other working groups [17, 28], as these investigators defined the relative recovery coefficients of the 37-mm sphere to have 100% recovery.

A possible explanation of the observed bias in ^{18}F for large objects in the present study might relate to the number of (effective) iterations in the image reconstruction. However, calculated ^{18}F recovery coefficients of the 37-mm sphere were independent of the image reconstruction method. The various image reconstruction methods resulted in identical absolute recovery values for the largest sphere. In agreement with the literature [26, 27], the recovery coefficient decreased faster with decreasing sphere diameter for FBP-reconstructed images (Figs. 3 and 4) because the

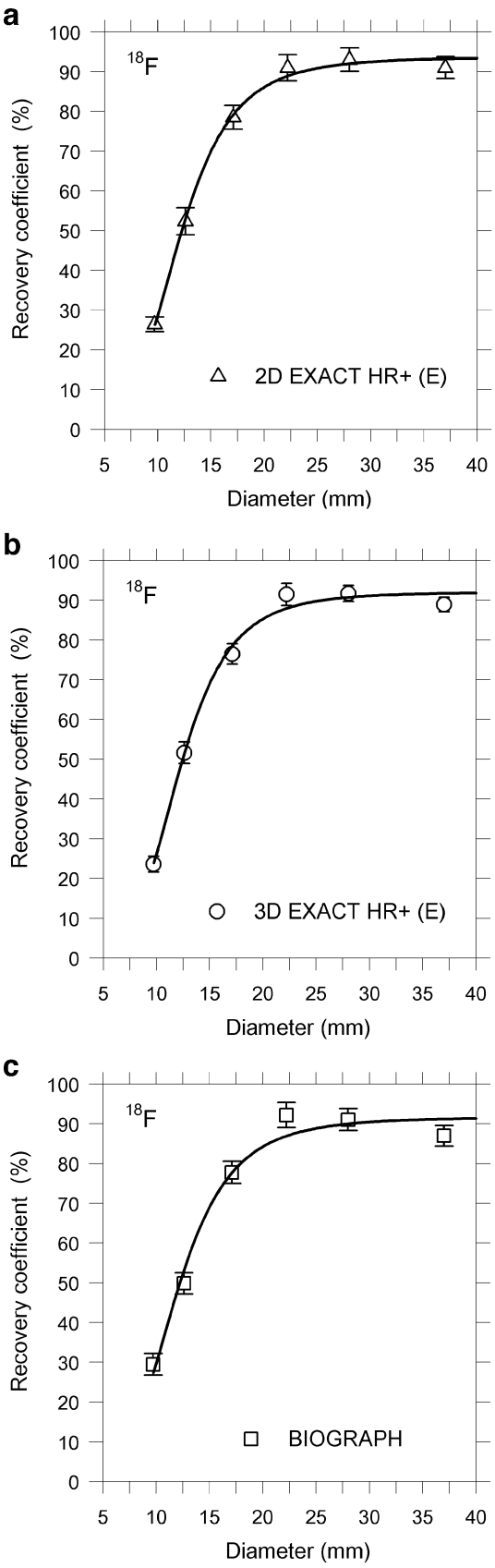

Fig. 5 Absolute recovery coefficients of ^{18}F for the EXACT HR$^+$ in 2D (**a**) and 3D modes (**b**) and BIOGRAPH PET systems (**c**) both located in Essen (E) measured with a cylinder phantom. Methodology is described in the caption of Fig. 2

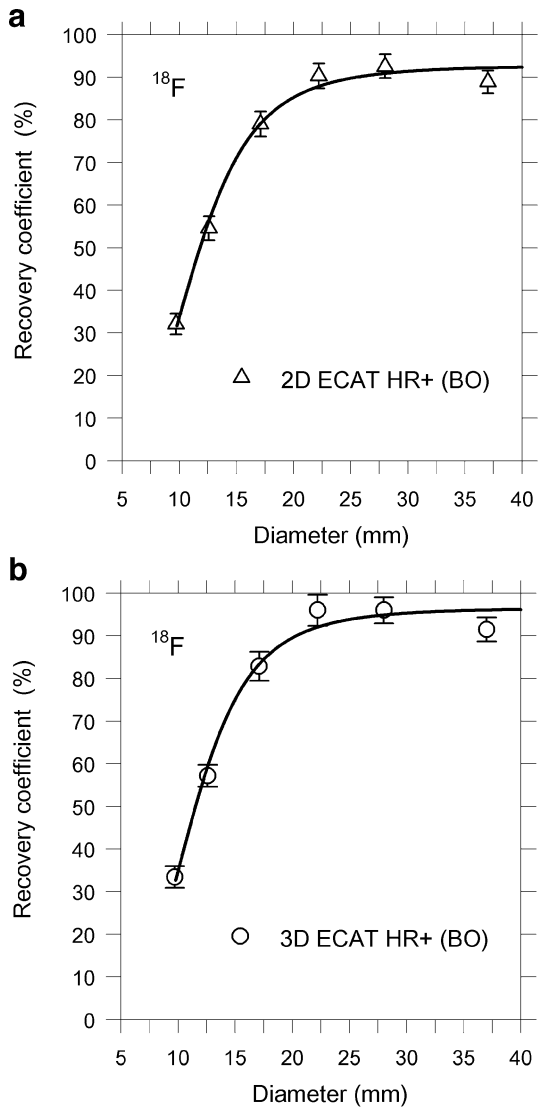

Fig. 6 Absolute recovery coefficients of ^{18}F for another EXACT HR^{+} located in Bad Oeynhausen (BO) measured with a cylinder phantom, acquired in 2D (**a**) and 3D modes (**b**). AW-OSEM 2×8 image reconstruction was used. Further methodological description is given in the caption of Fig. 2

measured activity concentration is generally underestimated compared to the concentration obtained with OSEM-reconstructed images.

This finding is indicative of a system-inherent bias. ^{18}F recovery measurement was performed on a different PET scanner. The GE ADVANCE PET system also contained bismuth germanate detectors. As shown in Fig. 7, the absolute recovery value for the largest sphere did not significantly deviate from 100%, that is, full recovery was reached, suggesting that the discrepancy indeed was system-specific. Since the GE ADVANCE PET system did not show the bias in ^{18}F, one has to conclude that the described procedure has to be done on every PET system with which one intends to do quantitative imaging.

The observed system-inherent bias in ^{18}F (deviation of ≈10%) may be associated with the observation of Lubberink and colleagues [28] that the EXACT HR^{+} PET scanner is not linear. These investigators measured the hot spot recovery coefficient (*HSRC*) and cold spot recovery coefficient (*CSRC*) and used the theoretical relationship, *HSRC = 1-CSRC*, for a system that responds linearly [24]. Lubberink and colleagues [28] showed with ^{18}F that the measured *HSRC* and *CSRC* deviated from the theoretical relationship. The authors of the present study also performed this test of system linearity using images of the body phantom that were reconstructed via FBP algorithm (linear operation). We substantiated the non-linear behavior of both EXACT HR^{+} scanners and of the BIOGRAPH PET

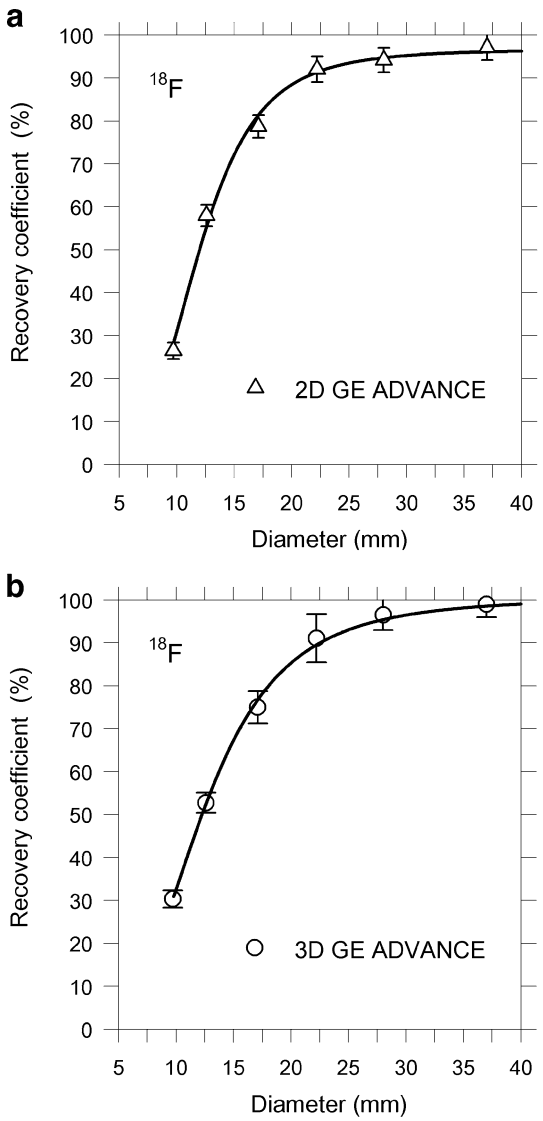

Fig. 7 Absolute recovery coefficients of ^{18}F for a GE ADVANCE PET system measured with a cylinder phantom, acquired in 2D (**a**) and 3D modes (**b**). OSEM 4×16 image reconstruction was used (see text). Further methodological description is given in the caption of Fig. 2

Table 3 Validating the recovery correction method using the body phantom prepared under typical conditions observed in lesion ^{124}I PET dosimetry in DTC*

Tomograph, mode	Diameter in mm, (*RC* used)†	Δ in %, scan 1	Δ in %, scan 2	Δ in %, scan 3	Δ in %, mean (*RSD*)‡
EXACT HR$^+$, 2D	9.7 (19.7)	0.2	5.9	−1.5	1.5 (3.9)
	12.6 (37.6)	4.1	−0.8	16.2	6.5 (8.6)
	17.1 (60.5)	−3.7	−0.1	−5.2	−3.0 (2.7)
	22.2 (73.5)	−6.1	−13.3	−2.6	−7.3 (5.4)
	28.0 (79.6)	5.3	−1.9	−2.6	0.3 (4.4)
	37.0 (82.8)	0.5	−0.7	2.4	−0.9 (1.5)
EXACT HR$^+$, 3D	9.7 (21.9)	−0.3	−7.4	−19.6	−8.9 (10.1)
	12.6 (39.1)	−8.7	2.7	−5.1	−3.7 (5.8)
	17.1 (59.1)	−7.7	−2.1	−6.2	−5.3 (2.9)
	22.2 (70.0)	−3.3	−1.2	−3.8	−2.8 (1.4)
	28.0 (75.2)	1.0	3.0	0.1	1.4 (1.5)
	37.0 (77.9)	−2.3	−3.0	0.1	−1.7 (1.6)
BIOGRAPH, 3D	9.7 (19.9)	−24.4	−32.5	−5.1	−20.7 (13.9)
	12.6 (39.4)	−8.5	−9.0	−8.5	−8.7 (0.3)
	17.1 (62.1)	−4.8	−1.9	−6.4	−4.4 (2.4)
	22.2 (73.2)	6.6	6.0	0.5	4.1 (4.1)
	28.0 (77.6)	8.8	9.0	3.0	6.9 (3.6)
	37.0 (79.7)	3.6	3.8	3.2	3.1 (0.5)

*Individual deviations (in percentage of the prepared ^{124}I activity concentration) between the recovery-corrected and prepared activity concentrations are given for the three consecutive scans numbered from 1 through 3. † Sphere inner diameter. The fitted ^{124}I recovery coefficients (in percentage) used are given in parentheses. ‡ Percentage deviation of the mean value of the recovery-corrected activity concentration (three scans) from the prepared activity concentration. The corresponding relative standard deviation (*RSD*) in percentage of the prepared activity concentration is given in parentheses.

system used in the present study (data not shown). Thus, this non-linear behavior is an indication that corrections such as those for attenuation and, especially, scatter do not perform accurately. Further investigations are necessary to elucidate the main cause of the system non-linearity of response and to clarify the source of errors for the observed bias in ^{18}F recovery.

Another issue in the present study was to validate the accuracy of the recovery correction method including reproducibility measurements under clinical imaging conditions typically found in ^{124}I PET of DTC patients. Using a GE ADVANCE PET scanner, Eschmann and colleagues [2] reported for ^{124}I phantom measurements in 2D mode an inaccuracy of about 10%. Similar inaccuracies were found in the present study. Specifically, the maximum uncertainty range of about ±10% was found for spheres ≥12.6 mm in diameter for the EXACT HR$^+$ and BIOGRAPH PET systems (Table 3). Obviously, the limitation of the recovery correction method applied under clinical conditions was reached for the smallest sphere (9.7 mm) that is in agreement with published data [9]. More specifically, even if the volume of the lesion can be determined very accurately, the applicability of the recovery correction method is limited for lesions <12.6 mm (≈1.5 times the scanner resolution).

Partial volume correction based on measured recovery coefficients is possible for simple geometric objects like spheres and for diameters larger than 1.5 times the scanner resolution. Such correction is, however, non-trivial to perform for objects that, for example, significantly deviate from spherical shape or possess inhomogeneous activity distribution. However, recovery correction as currently applied [24] is nonetheless a reasonable way to a more accurate quantification compared to that obtained with gamma-camera based dosimetry [29] and is in most cases acceptable to estimate the absorbed dose of subsequent ^{131}I therapy using serial ^{124}I PET(/CT) imaging such as in thyroid cancer.

Conclusion

In ^{124}I PET dosimetry, recovery correction must be applied even to large lesions, but is a reasonable way to a more accurate estimation of the absorbed dose of ^{131}I radioiodine therapy to metastases of thyroid cancer than that obtained using gamma cameras. Recovery correction is effective in lesions as small as approximately 1.5 times the *FWHM* (in our case, ≥12.6 mm). Using the EXACT HR$^+$ PET scanner, an unidentified source of bias in ^{18}F quantification was demonstrated and appeared to be system-specific. Therefore, to ensure accurate quantification, it is strongly recommended to determine the absolute recovery coefficients of each radionuclide and PET system used.

Acknowledgments The authors would like to thank Dr. Stefan P. Müller (Universität Duisburg-Essen, Germany) and Dr. Hartwig Newiger (Siemens Medical Solutions, Erlangen, Germany) for helpful comments and discussions. Furthermore, we are indebted to Robert J. Marlowe (Jersey City, NJ, USA) for critically reviewing the paper.

References

1. Erdi YE, Macapinlac H, Larson SM, Erdi AK, Yeung H, Furhang EE, et al. Radiation dose assessment for I-131 therapy of thyroid cancer using I-124 PET imaging. Clin Positron Imaging 1999;2:41–6.
2. Eschmann SM, Reischl G, Bilger K, Kupferschläger J, Thelen MH, Dohmen BM, et al. Evaluation of dosimetry of radioiodine therapy in benign and malignant thyroid disorders by means of iodine-124 and PET. Eur J Nucl Med 2002;29:760–7.
3. Sgouros G, Kolbert KS, Sheikh A, Pentlow KS, Mun EF, Barth A, et al. Patient-specific dosimetry for I-131 thyroid cancer therapy using I-124 PET and 3-dimensional-internal dosimetry (3D-ID) software. J Nucl Med 2004;45:1366–72.
4. Freudenberg LS, Bockisch A, Jentzen W. Iodine-124 PET dosimetry and PET/CT imaging in differentiated thyroid cancer. In: Biersack HJ, Grünwald F, editors. Thyroid cancer. Heidelberg - New York: Springer Verlag, 2005. 127–38.
5. Bockisch A, Freudenberg L, Rosenbaum S, Jentzen W. I-124 in PET imaging: impact on quantification, radiopharmaceutical development and distribution. Eur J Nucl Med Mol Imaging 2006;33:1247–8.
6. Freudenberg L, Jentzen W, Görges R, Petrich T, Marlowe RJ, Knust J, et al. I-124 PET dosimetry in advance differentiated cancer. Nuklearmedizin 2007;46:121–8.
7. Hoffmann EJ, Huang SC, Phelps ME. Quantitation in positron emission tomography: 1. Effect of object size. J Comput Assist Tomogr 1979;3:299–308.
8. Kessler RM, Ellis JT Jr, Eden M. Analysis of emission tomographic scan data: limitations imposed by resolution and background. J Comput Assist Tomogr 1984;8:514–22.
9. Geworski L, Knoop BO, Levi de Cabrejas M, Knapp WH, Munz DL. Recovery correction for quantification in emission tomography: a feasibility study. Eur J Nucl Med 2000;27:161–9.
10. Beattie BJ, Finn RD, Rowland DJ, Pentlow KS. Quantitative imaging of bromine-76 and yttrium-86 with PET: a method for the removal of spurious activity introduced by cascade gamma rays. Med Phys 2003;30:2410–23.
11. Herzog H, Tellmann L, Qaim SM, Spellberg S, Schmid A, Coenen HH. PET quantitation and imaging of the non-pure positron-emitting iodine isotope I-124. Appl Radiat Isot 2002;56:673–9.
12. Pentlow KS, Graham MC, Lambrecht RM, Cheung NK, Larson SM. Quantitative imaging of I-124 using positron emission tomography with applications to radioimmunodiagnosis and radioimmunotherapy. Med Phys 1991;18:357–66.
13. Pentlow KS, Graham MC, Lambrecht RM, Daghighian F, Bacharach SL, Bendriem B, et al. Quantitative imaging of iodine-124 with PET. J Nucl Med 1996;37:1557–62.
14. Robinson S, Julyan PJ, Hastings DL, Zweit J. Performance of a block detector PET scanner in imaging non-pure positron emitters - modeling and experimental validation with I-124. Phys Med Biol 2004;49:5505–28.
15. Knust EJ, Dutschka K, Weinreich R. Preparation of I-124 solutions after thermodistillation of irradiated $^{124}TeO_2$ targets. Appl Radiat Isot 2000;52:181–4.
16. Weinreich R, Knust EJ. Quality assurance of iodone-124 produced via the nuclear reaction ^{124}Te(d, 2n)^{124}I. J. Radioanal Nucl Chem Lett 1996;213:253–61.
17. Adam LE, Zaers J, Ostertag H, Trojan H, Bellemann ME, Brix G. Performance evaluation of the whole-body PET scanner ECAT EXACT HR$^+$ following the IEC standard. IEEE Trans Nucl Sci 1997;44:1172–9.
18. Beyer T, Townsend DW, Brun T, Kinahan PE, Charron M, Roddy R, et al. A combined PET/CT scanner for clinical oncology. J Nucl Med 2000;41:1369–79.
19. DeGrado TR, Turkington TG, Williams JJ, Stearns CW, Hoffman JM, Coleman RE. Performance characteristics of a whole-body PET scanner. J Nucl Med 1994;35:1398–406.
20. Lewellen TK, Kohlmyer SG, Miyaoka RS, Kaplan MS, Stearns CW, Schubert SF. Investigation of the performance of the General Electric ADVANCE positron emission tomograph in 3D mode. IEEE Trans Nucl Sci 1996;43:2199–206.
21. Schötzig, U. und Schrader, H.: Halbwertszeiten und Photonen-Emissionswahrscheinlichkeiten von häufig verwendeten Radionukliden. PTB-Bericht PTB-Ra-16/5, Braunschweig, 2000.
22. National Electric Manufactures Association. NEMA Standards Publication NU 2-2001: Performance measurements of positron emission tomographs. 2001; 1–40. Rosslyn, VA, National Electric Manufactures Association. NEMA Standards Publication NU 2-2001.2001.
23. International Standard IEC 61675-1: Radionuclide imaging devices - characteristics and test conditions - Part 1: Positron emission tomographs. International Eletrotechnical Commission. Geneva, 1998.
24. Knoop BO, Geworski L, Hofmann M, Munz DL, Knapp WH. Use of recovery coefficients as a test of system linearity of response in positron emission tomography. Phys Med Biol 2002;47:1237–54.
25. Levin CS, Hoffman EJ. Calculation of positron range and its effect on the fundamental limit of positron emission tomography system spatial resolution. Phys Med Biol 1999;44:781–99.
26. Ramos CD, Erdi YE, Gonen M, Riedel E, Yeung HW, Macapinlac HA, et al. FDG-PET standardized uptake values in normal anatomical structures using iterative reconstruction segmented attenuation correction and filtered back-projection. Eur J Nucl Med 2001;28:155–64.
27. Schoder H, Erdi YE, Chao K, Gonen M, Larson SM, Yeung HW. Clinical implications of different image reconstruction parameters for interpretation of whole-body PET studies in cancer patients. J Nucl Med 2004;45:559–66.
28. Lubberink M, Schneider H, Bergstrom M, Lundqvist H. Quantitative imaging and correction for cascade gamma radiation of ^{76}Br with 2D and 3D PET. Phys Med Biol 2002;47:3519–34.
29. Jentzen W, Schneider E, Freudenberg L, Eising EG, Gorges R, Muller SP, et al. Relationship between cumulative radiation dose and salivary gland uptake associated with radioiodine therapy of thyroid cancer. Nucl Med Commun 2006;27:669–76.